Received: 24 November 2023 | Revised: 7 June 2024 | Accepted: 22 July 2024

DOI: 10.1111/bre.12892

Basin Research IAS EAGE WILEY

RESEARCH ARTICLE

Short-term climatic oscillations versus long-term delta propagation: Controls on sand transport into the deep Levant Basin since the Pliocene

Ido Sirota[1,2] | **Yoav Ben Dor**[1] | **Zohar Gvirtzman**[1,3]

[1]Geological Survey of Israel, Jerusalem, Israel

[2]Section Climate Dynamics and Landscape Evolution, GFZ German Research Centre for Geosciences, Potsdam, Germany

[3]The Fredy & Nadin Herrman Institute of Earth Sciences, The Hebrew University, The Edmond J. S Afra Campus—Givat Ram, Jerusalem, Israel

Correspondence
Ido Sirota, Geological Survey of Israel, 32 Yesha'ayahu Leibowitz, Jerusalem 9692100, Israel.
Email: idosir@gfz-potsdam.de

Funding information
BIRD Foundation

Abstract

Sand transport and its deposition in deep marine basins are controlled by diverse climatic, tectonic, physiographic and oceanographic processes. Disentangling the impact of each of these drivers on the sedimentary record is a fundamental challenge in the study of source to sink systems. In this study, we investigate seismic and borehole data by combining statistical and spectral analyses to identify the factors controlling sand deposition in the deep Levant Basin (Eastern Mediterranean) during the Pliocene–Quaternary (PQ). We interpret the sand content in boreholes from gamma ray (GR) logs and identify two major trends in sand/shale ratios. On a million-year scale, we demonstrate that since the Early Pliocene (5.3 Ma), sand content gradually increased until it formed a ca. 100 m thick and widespread sheet of sand at the top of the section. On a shorter time scale, we identify oscillations in sand content depicting significant power of periodic components at the 350–450 ky, 90–150 ky and 10s ky bands. The long-term increase in sand content reaching the deep Levant Basin is interpreted as a result of the Nile Delta propagation, which had continuously shortened the distance between the edge of the Nile delta that is the source of sand, and the deep Levant Basin. The superimposed short-term oscillations are interpreted as Milanković cycles, reflecting hydroclimatic oscillations of water and sediment discharge into the Eastern Mediterranean Sea by the Nile River. This demonstrates the hydroclimatic control on sand deposition in the deep Levant Basin. Our observations are consistent with the development of a submarine channel system along with the accretion of the Nile delta, which may have served as a pathway for sand delivery via high-energy turbidity currents that reached the Levant Basin.

KEYWORDS

deep sand deposition, source to sink systems, the Levant Basin, the Nile Delta, wavelength analysis

1 | INTRODUCTION

Rhythmic patterns commonly characterize deep marine sedimentary records (Hilgen et al., 1993; Hilgen & Langereis, 1989; Lourens et al., 1996; Weedon et al., 1999; Weedon & Jenkyns, 1999; Wu et al., 2012). These rhythmic patterns may be expressed by lithological, chemical, isotopic, faunal and physical characteristics (Erba et al., 1992; Kelly, 1992), and commonly correspond to astronomical forcing known as 'Milanković cycles' (Hilgen et al., 2015; Imbrie & Imbrie, 1980; Shackleton, 2000; Zachos et al., 2001). These astronomical cycles show increased power in periodicities of 19–24 ky (precession), 41 ky (obliquity), 95–131 ky (short eccentricity) and 405 ky (long eccentricity) (Hays et al., 1976; Meyers & Malinverno, 2018; Waltham, 2015).

One type of these rhythmic patterns includes alternations between shale- and sand-rich units, which are originated by fluctuations in the transport of sand over great distances by rivers (source) into deep marine basins (sink; e.g. Romans et al., 2016), combined with the impact of diverse internal depositional processes (e.g. Gong et al., 2021; Hajek & Straub, 2017). Those processes are commonly attributed to two categories. (i) *External (allogenic) effects* controlled by climatic and tectonic processes. These include, for example, variations in sediment and water supply (Rohling et al., 2015), sediment composition and provenance localities (Ben Dor et al., 2018; Gardosh et al., 2008; Macgregor, 2011; Zilberman & Calvo, 2013). (ii) *Internal (autogenic) effects* related to the physiography of the sedimentary basin and inherent marine processes. These include gravity-driven transport (e.g. turbidity currents; Mulder & Cochonat, 1996; Shanmugam et al., 1993; Stow & Smillie, 2020; Strachan et al., 2016), along-strike current-driven transport (Garzanti et al., 2014; Stow & Smillie, 2020; Weldeab et al., 2002), dynamics of water masses and marine circulation (Rohling et al., 2015; Stratford et al., 2000), eustatic fluctuations (Muto & Steel, 2002; Sweet et al., 2020; Zecchin et al., 2015) and the physiographical evolution of the basin (Zucker et al., 2021).

Distinguishing external from internal controls on the accretion of deep-basin sedimentary sections is difficult, and identifying mechanistic links between variations in sand proportion and depositional processes controlling it is particularly challenging. One possibility is to search for periodicities that fit previously reported cycles such as precession, obliquity, or eccentricity in palaeoclimatic proxies, which may indicate climatic control over sediment deposition (Fang et al., 2020; Martin et al., 2002), and can be correlated with other sedimentary records (Liu et al., 1999). Various methods of time series analysis, wavelet analysis and running tests are commonly applied to reveal significant periodicities in rhythmic sedimentary sequences (e.g. Ben Dor et al., 2021; Donges et al., 2011; Lau & Weng, 1995; Liu et al., 1999; Pickering et al., 1999; Schulte, 2019; Welch, 1967; Wu et al., 2012). These methods proved to be useful for identifying dominant oscillatory components and for linking depositional processes and environmental forcing (Blackman & Tukey, 1958; Ghil et al., 2002; Grinsted et al., 2004; Torrence & Compo, 1998).

Highlights

1. First well record of the 100 s-m-thick Plio-Quaternary deep Levant Basin section.
2. Sand–shale ratio inferred from Gamma Ray logs illustrate changes in terrigenous supply.
3. Long-term (Myr) increase in sand content expresses Nile Delta propagation.
4. Short-term (10s–100s ky) Quasi-Milinković sand/shale oscillations express hydroclimate control.

The main question this study addresses is: *What are the internal and external controls on sand/shale alternations in the deep-marine siliciclastic Levant Basin? Can these internal versus external controls be distinguished in the stratigraphic record?* To answer these questions, we explore the Pliocene–Quaternary (PQ) section of the deep Levant Basin (Eastern Mediterranean) as a case study, using well logs from four boreholes. This section is a part of one of the largest source-to-sink systems on Earth, the Nile River, which transports substantial volumes of sand from Northeast Africa to the Eastern Mediterranean. Additionally, the section contains valuable information about the dynamics of the Nile River and adds up to relatively few examples of the Pliocene and lower Pleistocene period from deep marine basin records, worldwide (De Schepper et al., 2014).

2 | REGIONAL SETTING

The Nile River is the main supplier of terrigenous sediment into the Levant Basin. It is one of the longest rivers in the world, draining ca. 3×10^6 km^2 of northeast Africa and flowing northwards along ca. 6700 km into the Eastern Mediterranean (Figure 1a). Its mean annual water discharge is ca. 90 km^3 year^{-1} (Eltahir, 1996), where more than half is derived from the Blue Nile (draining the Ethiopian Plateau), ca. 30% from the White Nile (draining the equatorial lake plateau), whereas the remaining water supply is from the Atbara River (draining the northern fringe of the Ethiopian Plateau)

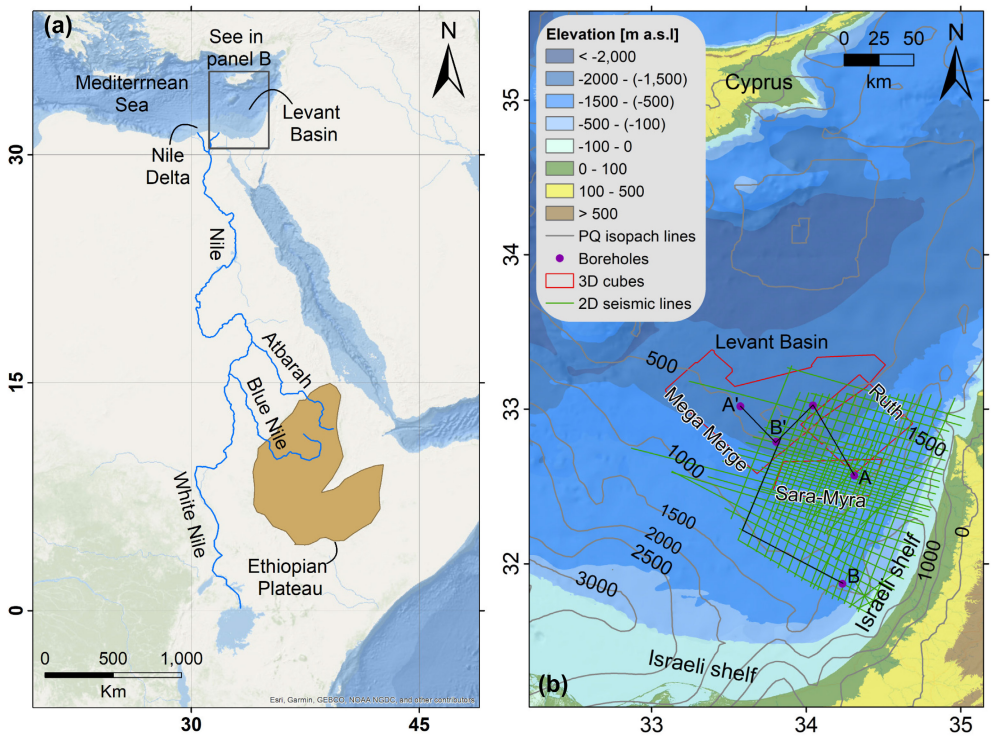

FIGURE 1 Location map. (a) Nile River sources in tropical Africa (White Nile) and the Ethiopian Plateau (Blue Nile and Atbarah). (b) The Levant Basin.

(Ahmed & Ismail, 2008; Sutcliffe & Parks, 1999). While the discharge of the White Nile is constant throughout the year, the Blue Nile experiences a nearly fivefold increase in water discharge during the wet monsoon season in the Ethiopian Plateau (June–September; Ahmed & Ismail, 2008). Interestingly, more than 90% of the annual sediment yield of the Nile is derived from the Ethiopian Plateau (Garzanti et al., 2006). Thus, water and sediment discharge of the Nile are highly sensitive to hydroclimatic fluctuations at the Ethiopian Plateau (Ahmed & Ismail, 2008).

The Nile River provides sediments to three main sedimentary units in the study area: the Nile Delta, the Levant deep basin, and the nearby continental shelf (another major sink outside the study area is the Herodotus Basin).

The Nile Delta is one of the world's largest sedimentary units (Figure 1a). Its modern delta started accumulating after the Messinian Salinity Crisis (MSC), during which Mediterranean Sea level dropped by 0.5–1.5 km (Clauzon et al., 1996; Gargani & Rigollet, 2007; Gvirtzman et al., 2022; Kirkham et al., 2020), driving backward incision of the Nile River into the North African continental margin (Barber, 1981; Said, 1981). Since the Early Pliocene, after the rejuvenation of the Mediterranean Sea to global sea level, a large volume of sediments filled the incised Nile canyon, and started forming the Nile Delta, which have been prograding towards the Levant and the Herodotus deep basins since the Pliocene (Figure 1). Presently, the Nile Delta spreads ca. 200 km northwards of the mouth of the Messinian Nile canyon (near the city of Cairo), its area covers ca. 40,000 km^2, and its maximal thickness (PQ section) reaches >4 km (Macgregor, 2012; Zucker et al., 2020).

The Israeli continental shelf is considered a by-product of the Nile Delta, built by margin parallel sediment transport (Bookman et al., 2021; Marriner et al., 2012; Schattner et al., 2015; Zucker et al., 2021) that accreted a new continental shelf offshore Israel, reaching a thickness of ca. 1.5 km (Gvirtzman & Buchbinder, 1978; Steinberg et al., 2011; Zucker et al., 2021). Based on seismo- and biostratigraphic data, Elfassi et al. (2019) divided this section into four units, and demonstrated that the continental shelf started accumulating only during the Gelasian (1.8–2.6 Ma), that is, >2.5 Myr after the beginning of delta formation offshore Egypt. Modelling efforts of margin parallel sediment transport indicate that the Israeli shelf could have started forming only after the establishment of a continental shelf offshore Sinai (Zucker et al., 2021).

Levant basin sedimentary fill: The origin of the Levant sedimentary fill since the Upper Eocene to the Middle Miocene include two main potential sources: an eastern source from Arabia (Gardosh et al., 2008; Zilberman & Calvo, 2013) and a southern source from Africa (Gvirtzman et al., 2014; Macgregor, 2012;

Schattner, 2021; Steinberg et al., 2011; Zucker et al., 2021). It is accepted that the eastern contribution became negligible since the Upper Miocene due to the blocking of fluvial systems draining Arabia by the Dead Sea transform (Bar et al., 2016; Garfunkel, 1981). Thus, at least since the Pliocene, the Nile River is the main sediment supplier to the Levant Basin (Be'eri-Shlevin et al., 2014; Macgregor, 2012; Segev et al., 2006; Steinberg et al., 2011; Weldeab et al., 2002). Additionally, a part of the Nilotic sediments transported alongshore the Levant shelf is later transported into the deep basin (Schattner et al., 2015).

The sedimentary evidence for the Nile being the main sediment source of the deep Levant basin is further supported by the thinning of the PQ sedimentary fill northeastwards, from the Nile Delta towards the Levant basin (Steinberg et al., 2011). Moreover, seismic data show a set of channel systems within the PQ section, extending from the Nile Delta towards the deep Levant Basin as a potential pathway of sediment transport from the Nile to the Levant Basin (Niyazi et al., 2018; Sagy et al., 2020).

Currently, sedimentation in the Levant Basin comprises more than 90% terrigenous material complemented with a minor component of authigenic carbonates (Bookman et al., 2021; Gvirtzman & Buchbinder, 1978; Krom et al., 1999; Nir, 1984; Venkatarathnam & Ryan, 1971). Seismic data show that the thickness of the PQ section in the deep Levant basin (not including the Nile deep sea cone and not the Levant shelf) varies within a range of 500–1000 m (Sagy et al., 2020; Steinberg et al., 2011; Zucker et al., 2020).

3 | PURPOSE OF STUDY

So far, sedimentary studies of the deep Levant section from borehole data (logs and cuttings), focused on the Oligo-Miocene section associated with large hydrocarbon reservoirs (Needham et al., 2017; Torfstein & Steinberg, 2020) and on the Messinian evaporites related to the MSC (Feng et al., 2016; Gvirtzman et al., 2017; Manzi et al., 2018; Moneron & Gvirtzman, 2022; Zucker et al., 2021). However, the lithology of the PQ section in the deep basin that is directly related to the Nile River remained unknown. Here, we focus on sand transport to the deep basin. Our objectives are: (1) to characterize sand proportion along the Levant PQ section using well logs correlated with seismic reflection data, (2) to determine and investigate the timing and properties of sand/shale alternations along a transect of several boreholes recording N–S and E–W variations in sedimentation, and (3) to identify oscillatory components in the depositional record of the Levant basin and interpret them with respect to depositional processes controlling sand transport into the basin.

4 | METHODS, DATA AND MATERIALS

4.1 | Seismic data and age model

Three high-resolution 3D depth-migrated seismic reflection surveys with trace interval of 12.5 × 12.5 m for Mega Merge and Ruth and 12.5 × 25 m for Sara-Mira were used for seismic correlation. These surveys are Sara-Mira (2011, by Sewell & Associates Inc.), Ruth (2010, by Modiin Energy LP) and Mega-Merge (2012, by Fugro Seismic Imaging Inc.). Elfassi et al. (2019) used global and local biozonation schemes of planktonic foraminifera and calcareous nannofossil to determine bio-stratigraphic ages along the PQ section in numerous boreholes from the Israeli shelf (Figure 1b). Those boreholes were tied to key seismic horizons, which were dated using biostartigraphic data. The dated seismic horizons were then correlated across the basin, and specifically along a section between several key wells: Yam-West (on the Israeli shelf), Sara-1, Tamar-1, Dolphin 1, and Leviathan 1 (Figure 1b). The intersection of the dated horizons with the wells studied here, provide 4 ages constraints for each depth series: 5.33 Ma (top Messinian), 2.6 Ma (top of Unit 1), 1.8 Ma (top of Unit 2) and 0 Ma (seafloor). A linear interpolation was applied between these age anchors. Although this age model is limited to four anchor points, it provides a substantial improvement compared with the preceding model, which was based two anchor points (5.5 and 0 Ma), and was available a few years ago.

4.2 | Well logs data

Gamma ray (GR) and resistivity (Res) logs of four boreholes (Sara 1, Tamar 1, Dolphin 1 and Leviathan 1) were used to characterize relative sand proportion. Because cuttings or cores are unavailable, we have to rely on GR logs as the next best available option for interpreting sand/shale ratio in our study area. GR logs are considered to be the most direct indication of the sand/shale ratio in hemipelagic/siliciclastic environments, which is also applicable in this case since the Eastern Mediterranean is considered a siliciclastic basin (Garzanti et al., 2015; Nir, 1984; Weldeab et al., 2002), where high GR values reflect low sand proportion and vice versa (Baker Atlas, 2002; Ellis & Singer, 2008). An evaluation of the sand/shale ratio is carried out using the linear scaling of the GR values

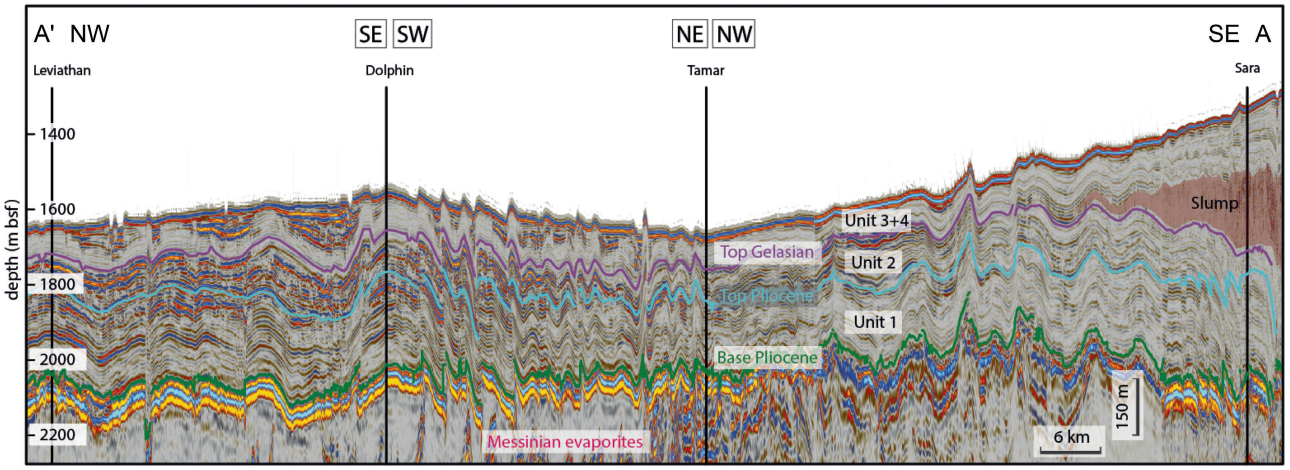

FIGURE 2 A seismic transect AA′ crossing Levant Basin through all the investigated boreholes. The division of the Pliocene-Quaternary section into sub-units based on Elfassi et al. (2019).

used to calculate the shaliness index (Equation 1; Ellis & Singer, 2008).

$$I_{GR}\,(\%) = \left(\frac{\gamma_i - \gamma_{min}}{\gamma_{max} - \gamma_{min}}\right) \times 100 \qquad (1)$$

where I_{GR} is the percentage of shale in the sediments, γ_{log} is the in situ GR reading, γ_{min} is the minimum value of GR reading along the borehole and γ_{max} is the maximum value of GR reading measured along the borehole. The minimum reading may be simplistically interpreted as the cleanest end-member (0% shale), and the maximum reading represents the shale end-member (100% shale). It is important to note that this index does not address other sediment types (e.g. carbonates, sulphates and evaporites), which have been shown to be of negligible importance in the Eastern Mediterranean (Bookman et al., 2021; Gvirtzman & Buchbinder, 1978; Krom et al., 1999; Nir, 1984; Venkatarathnam & Ryan, 1971), and are thus assumed to be negligible in the boreholes investigated in this study. Here, we use this index to evaluate relative variations in sand deposition across the Levant Basin during the PQ, rather than obtaining the absolute sand content. Noteworthy, due to technical limitations at the upper 70–100 m of each borehole, well logs in this interval are considered of low quality and therefore are not included in the following analyses.

4.3 | Spectral analysis

High-resolution GR records of four boreholes were studied using multiple statistical methods to analyse sand/shale alternations and to identify oscillatory components. Due to the limited quality of the well logs at the upper part of the borehole, only the interval between 5.33 and 1.8 Ma was analysed. Before the analyses of the Dolphin-1 well, missing data (33% of the record) were imputed using singular spectrum analysis (Kondrashov & Ghil, 2006), to reduce abruptions to the spectral properties of the series. Because the well data are anchored to depth, each series was resampled and transformed into a time series, based on the dated horizons; finally, all series are presented in 1 ky intervals.

Spectral analyses are used to detect oscillatory signals reflecting rhythmic forcing over sedimentation that may provide insights and implications on the processes involved in the accumulation of sedimentary sequences (e.g. Blackman & Tukey, 1958; Lomb, 1976; Muller & MaCdonald, 2002; Trauth, 2021; Welch, 1967 and references therein). Wavelet analysis is another useful tool for estimating the spectral properties of a time series, and is often used to detect non-stationary oscillatory behaviour in environmental records (Debret et al., 2007; Witt & Schumann, 2005). Unlike the 'bulk' spectral approaches, wavelet analysis provides more detailed insights into changes in the spectral properties of the series and their evolution, by identifying changes in the spectral power density of different spectral bands over time. This is especially useful for exploring geological records, which are often affected by multiple irregular and non-stationary processes (e.g. Ben Dor et al., 2021; Schulte, 2016). It therefore provides more detailed insights for identifying partial, irregular and non-stationary oscillatory components in the record (Grinsted et al., 2004; Lau & Weng, 1995; Torrence & Compo, 1998). Wavelet analyses were carried out with the Morlet wavelet function after normalizing the data to zero mean and unit SD. The significance of the wavelet power was determined at $\alpha = 0.1$ against red noise simulated using a lag-1 autoregressive process (AR[1]) using the cumulative area-wise approach

(Schulte, 2016, 2019). The background levels were determined by multiple background alpha levels (0.5, 0.6, 0.7, 0.8 and 0.9), and the significance of the global wavelet spectra was determined using the arc-wise significance at $\alpha = 0.1$ (Schulte, 2019).

5 | RESULTS

5.1 | Seismo- and Chronostratigraphy

Figure 2 presents seismic section AA′ connecting the four deep basin wells analysed in this study (location in Figure 1b). The absolute ages of the seismic units are based on Elfassi et al. (2019), who dated the seismic reflectors using biostratigraphic data on well records in the continental shelf. Extension of the dated horizons from the shelf to the deep basin is based on section BB′ (location in Figure 1b). Here, we follow the numbering of the seismic units by Elfassi et al. (2019), without differentiating units 3 and 4, because unit 4 is thin and therefore hard to distinguish in the deep basin.

Seismic unit 1 comprises the entire Pliocene and is bounded by the green (base) and light blue (top) horizons. The base of unit 1 (green horizon) is located at the top of the Messinian evaporites, which have a strong seismic reflection across the basin and are thus easily identified. Unit 1 is a package of light and sub-horizontal reflectors maintaining a nearly constant thickness of 150–250 m. Unit 2 is composed of a seismic facies similar to unit 1, but exhibit stronger seismic reflections in the deep basin. Unit 3+4 are composed of a nearly transparent (reflection-less) layer of constant thickness, at the base, covered by a variegated layer with strong reflections depicting significant thickness variations (thick in synclines and thin in anticlines). These variations indicate syn-tectonic deposition marking the initiation of the circum-Nile deformation belt (CNDB, Ben Zeev & Gvirtzman, 2020; Gvirtzman et al., 2015; Zucker et al., 2020). To the east, near Sara borehole, unit 3+4 contain a thick slump, named the Israeli Slump Complex (ISC; Elfassi et al., 2019; Martinez et al., 2005;Schattner & Lazar, 2016). The ISC pinches out west of Sara 1 borehole and is absent in the deep basin (Figure 2).

By tying three dated seismic horizons in the Yam-West borehole (Base Pliocene, Top Pliocene and Top Gelasian; Elfassi et al., 2019) to the GR depth series of the deep Levant Basin boreholes, an age model was established for the PQ section at each borehole (Figure 3). The age model allows to determine deposition rates and investigate cyclicity in the stratigraphic record (Table 1). We divide the record into isochronic GR units and identify oscillatory components in the GR data (Section 5.4).

5.2 | Well logs data

GR and Res logs of four boreholes are shown in Figure 3 with a seismic image as a background illustrating the bedding. The GR values vary between 4 and 115 API in Leviathan; 5–67 API in Dolphin; 2–153 API in Tamar; and 13–198 API in Tamar. The GR values in the *Leviathan borehole* decrease up-section (Table 1) with nearly no peaks in unit 2 and the base of unit 3. The upper ca. 70 m of the section are characterized by low GR values with substantial variation. There is a general correlation between variations in the GR and Res values. The *Dolphin borehole* displays similar average GR values in units 1 and 2, however, low GR excursions occur at the top of unit 1 and at unit 2. The upper ca. 100 m of the section is characterized by very low GR values. There is a general correlation between variations in the GR and Res values. *Tamar and Sara boreholes* display relatively high GR values along units 1 and 2, with no significant interval of low GR values as observed in Leviathan and Dolphin boreholes. The upper ca. 100 m of the section in Sara, and the upper ca. 80 m in Tamar display very low GR values with large variations.

5.3 | Shaliness index

In general, the shaliness index indicates an increase in sand proportion (low shaliness) during the PQ across the Levant basin in all four boreholes (Figure 4). In the *Leviathan borehole* unit 1 (Pliocene) is mostly composed of shales with 11 thin sand intervals (1 m scale thickness; ca. 25% of the section). Unit 2 (Gelasian) is composed mostly of shales in its lower part and sand in its upper part, whereas units 3 and 4 (upper ca. 100 m of the section) are composed almost entirely of sand. In the *Dolphin borehole*, unit 1 (Pliocene) is composed almost entirely of shale (ca. 80%), with two sand units at its upper part (20 m thick each). Unit 2 (Gelasian) is composed of shale (ca. 75%) with a ca. 20 m sand unit at its middle part, and units 3 and 4 (upper ca. 90 m of the section) are composed almost entirely of sand (90%). In the *Tamar borehole*, units 1 and 2 (Pliocene–Gelasian) are composed almost entirely of shales with practically no sand units. The lower third of units 3+4 is composed of shales, while its upper two-thirds are composed of sand. At the *Sara borehole* units 1 and 2 (Pliocene–Gelasian) are composed mainly of shales (two-thirds of the section) with frequent thin sand units (m's scale thickness; one-third of the section), and units 3+4 are significantly thicker in these boreholes compared with the other boreholes due to a large slump interbedded within the sequence (see the Sara seismic section in Figure 3). The lower two-thirds of the section are predominantly composed of shales with several

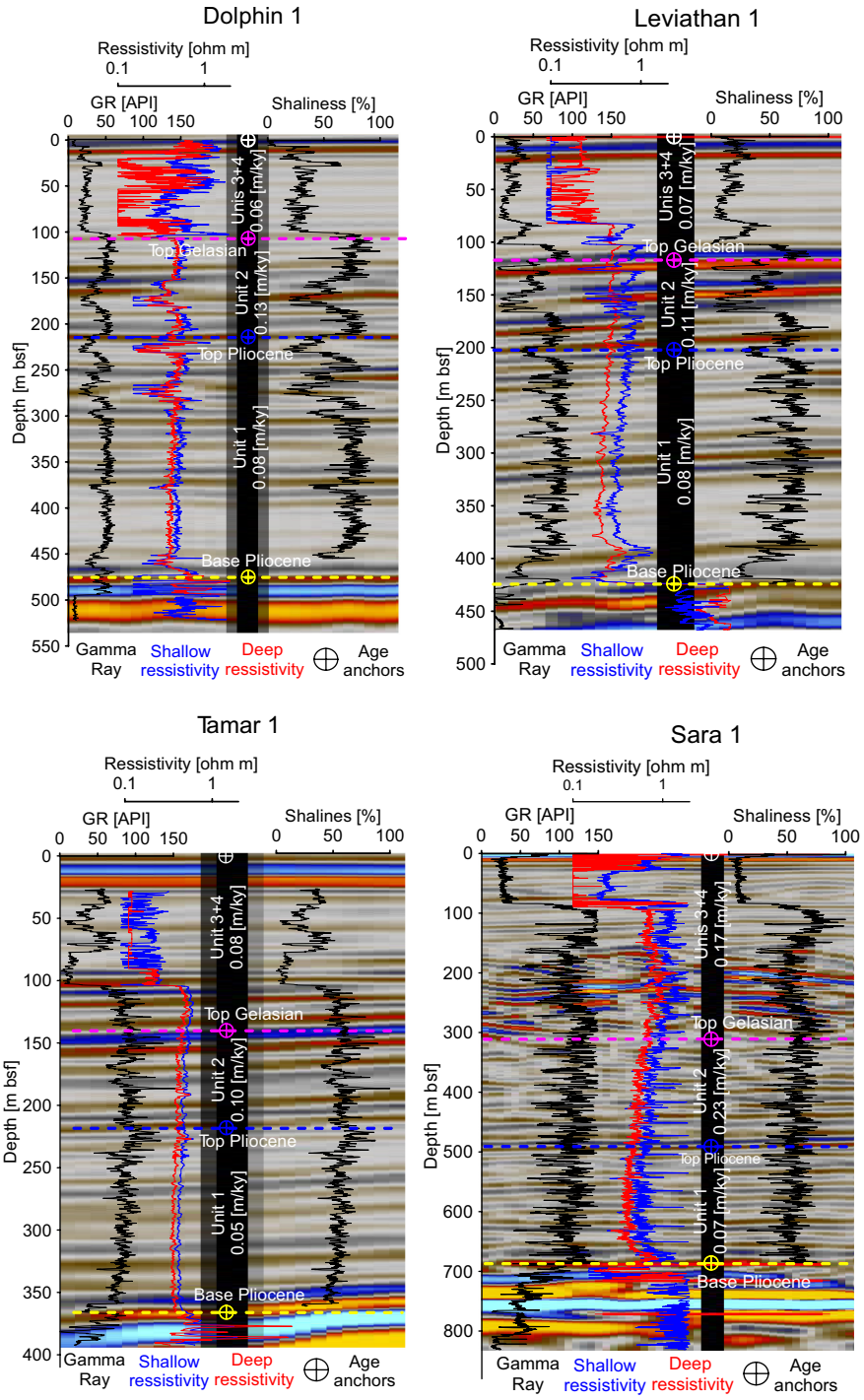

FIGURE 3 Seismic column, well logs and shaliness index of the four boreholes.

one-meter sand intervals within the slump segment of the section, and the upper one-third of the section (ca. 70 m) is composed of sand.

5.4 | Spectral analysis—oscillatory properties of siliciclastic deposition in the Levant basin

The wavelet analyses of the GR depth-time series from the four boreholes show clear oscillatory components in the Levant Basin Pliocene–Gelasian sedimentary record (Figures 5 and 6). The *Leviathan borehole* wavelet spectrum shows increased power at the 370–410 ky, 220–270 ky, 145–180 ky, 95–120 ky, 60–80 ky and ca. 37–42 ky bands, persistent during the entire Pliocene–Gelasian (Figure 5a). At the *Dolphin borehole*, increased power is observed at the 400–440 ky, 135–160 ky, 105–115, 60–70 ky and 10–35 ky bands. While the ca. 400 ky periodicity is characterized by high power over the entire Pliocene–Gelasian, the increases of power in bands of shorter periodicities are not as persistent, and show variations

TABLE 1 Gamma ray values and deposition rates at all boreholes along the PQ section.

GR logs (API)	Mean (API)			SD (API)			Deposition rates (m/ky)		
Borehole	Unit 1 (5.33–2.6 Ma)	Unit 2 (2.6–1.8 Ma)	Units 3 + 4 (1.8–0 Ma)	Unit 1 (5.33–2.6 Ma)	Unit 2 (2.6–1.8 Ma)	Units 3 + 4 (1.8–0 Ma)	Unit 1 (5.33–2.6 Ma)	Unit 2 (2.6–1.8 Ma)	Units 3 + 4 (1.8–0 Ma)
Sara 1	112	118	95	20	20	45	0.07	0.23	0.17
Tamar 1	84	91	51	13	14	29	0.05	0.1	0.08
Dolphin 1	45	45	24	11	11	9	0.08	0.13	0.06
Leviathan 1	69	52	30	19	23	21	0.08	0.11	0.07

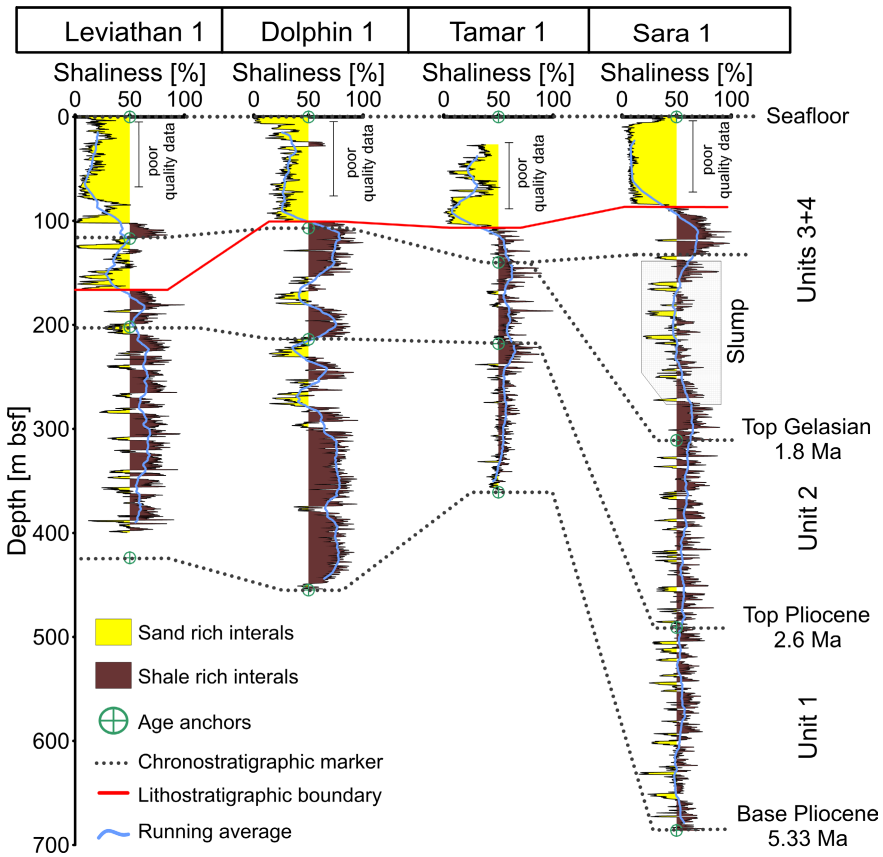

FIGURE 4 Stratigraphic correlation between the boreholes. 'Shaliness' index reflects the sand proportion along the Levant sedimentary fill at the four boreholes, and allow to explore spatiotemporal variations in the sand proportion of the Levant Basin during the PQ.

across the investigated time interval (Figure 5b). During the Lower Pliocene (5.33–3.8 Ma), 80–130 and 40–60 ky periodicities are dominant, whereas during the Upper Pliocene (3.8–2.6 Ma), 130–160 ky and 70 ky become dominant. During the Gelasian (2.6–1.8 Ma), periodicities of 100–130 ky, 30–40 ky and ca. 10 ky show increased power in addition to the ca. 400 ky time period (Figure 5b). The *Tamar borehole* is characterized by increased power of periodicities at the 400–440 ky, 220–250 ky, 105–130 ky, 80–90 ky and 30–55 ky bands (Figure 5c). These periodicities are not persistent over the Pliocene–Gelasian, and only the 80–140 ky band is dominant between 5.33 and 4 Ma, whereas between 4 and 2.6 Ma, the 200–300 ky, 120–130 ky, 80–90 ky and 40–60 ky bands become dominant. During the Gelasian (2.6–1.8 Ma), the 390–410 ky, 100–140 ky, 40–50 ky and ca. 10 ky bands are dominant. The *Sara borehole* spectrum shows increased power at the 350–450 ky, 240–270 ky, 100–120 ky, 80–90, 40–55 ky and 15–20 ky bands (Figure 5d). Between 5.33 and 3.5 Ma, the 300–400 ky, 90–140 ky and 40–80 ky are the dominant periodic components, whereas between 3.5 and 2.6 Ma, periodicities of bands 380–410 ky and 90–140 ky are dominant. During the Gelasian, 120–150 ky, 40–80 ky and ca. 10 ky periodicities become dominant.

To summarize, the GR depth series at the Levant Basin show an increased power of oscillatory components characterized by the 400–450 ky band, although the significance level of this band is low due to the limited series

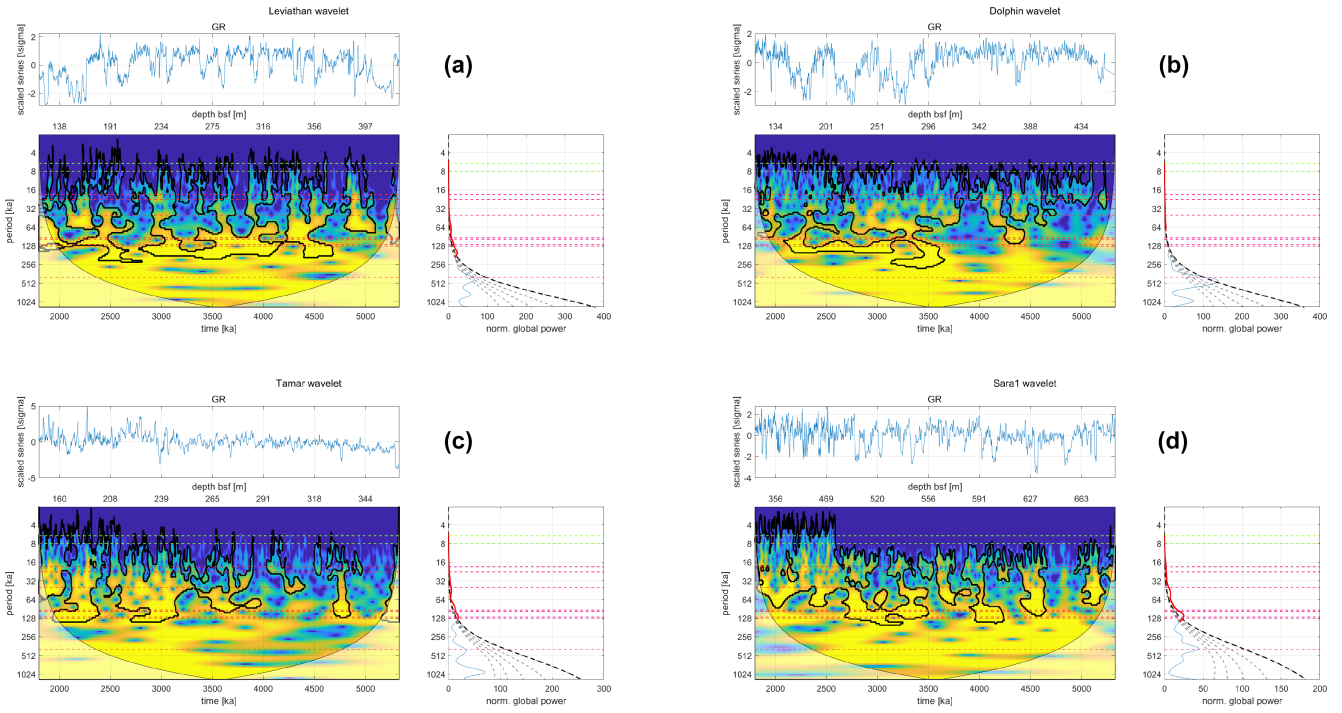

FIGURE 5 Spectral analyses of the Pliocene–Gelasian GR depth series at the four boreholes, (A) Leviathan, (B) Dolphin, (C) Tamar, and (D) Sara. The upper panel of each part shows the normalized series after *z*-scoring. The central part show the wavelet power spectrum (blue to yellow scale) as a function of period (*y*-axis) and time (*x*-axis) during the investigated section. The black line surrounds statistically significant areas. Right panel: The global power as a function of time period. Grey dashed lines indicate significance levels based on simulated red noise (50%–90%). Red segments indicate periodicities of statistically significant spectral power.

length. The power of the 90–150 ky band, on the other hand, is weaker, but is statistically significant. An additional oscillatory component characterized by increased power of the 10–10's ky band is also observed (Figure 6).

6 | DISCUSSION

6.1 | Sand/shales alternations in the Levant Basin Plio-Quaternary section

Highly variable GR records indicate significant and frequent temporal variations in the sand/shale ratio along the Levant Basin PQ sedimentary fill. Although the shaliness index (Figures 3 and 4) cannot be used for accurate comparison of sand proportion between the boreholes, it does reflect relative changes in sand proportion along each of them (Baker Atlas, 2002; Ellis & Singer, 2008). The Leviathan and Dolphin boreholes display increasing thickness and frequency of 'sandy' units up-section, while similar 'sandy units' are absent in the Pliocene–Gelasian section of Tamar and Sara (Figure 4). Although the upper 70–100 m at all boreholes suffer from poor quality data, this unit might indicate, with some caution, that a relatively 'sandy' unit covers the entire Levant Basin. The possibility that sediments in the Levant Basin originate from the Nile River is indeed consistent with the observation that enhanced sand deposition starts earlier in both Leviathan and Dolphin boreholes (Figure 4), which are closer to the Nile source relative to the Sara and Tamar boreholes (Figure 1b). The deposition of the top sand cover across the basin is approximately coeval with the development of a channel complex with a northeast orientation during the upper Quaternary (Sagy et al., 2020). Thus, it might indicate that sand is transported into the deep Levant Basin by channels as was previously observed at the Western Nile slope (Cross et al., 2009; Samuel et al., 2003) and additional regions (Babonneau et al., 2010).

Sand deposition seems to bear little implications on variations in deposition rates. For example, deposition rates increase in all four boreholes from unit 1 to unit 2, especially in Sara and Tamar, although sand proportion increases up-section in Leviathan and Dolphin. This might indicate that increasing sand proportion results from decreasing shale content, resulting in an overall decreased deposition rate. The deposition rate in units 2 and 3+4 in Sara is twice as high compared with the other boreholes. In unit 3+4, most of this difference is explained by a thick slump within the section that is associated with the ISC (Figures 3 and 4; Martinez et al., 2005; Schattner & Lazar, 2016). However, during the deposition of unit 2, this difference can be

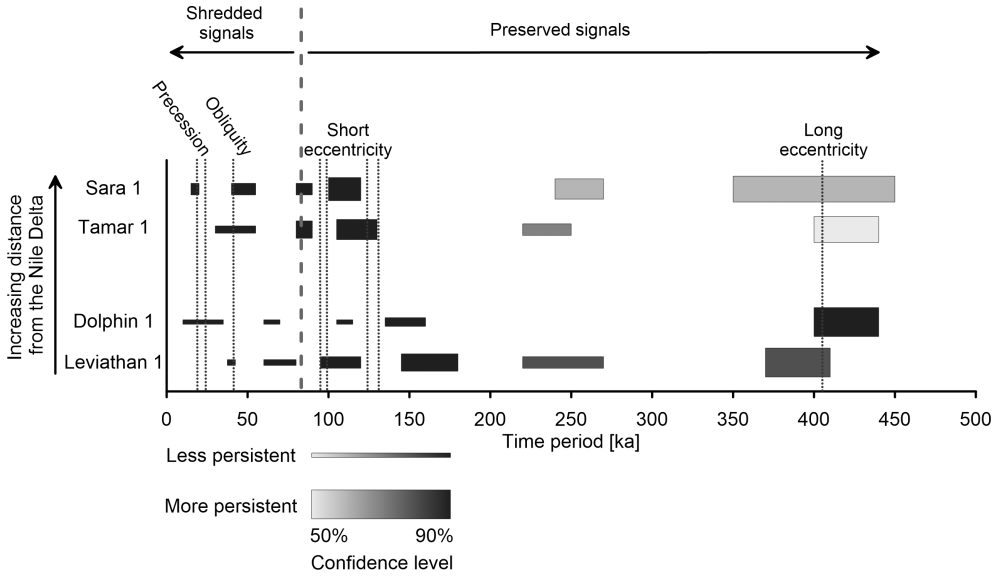

FIGURE 6 Time periods of increased wavelet spectra of the Pliocene–Gelasian section of the four boreholes. Significance level of each range of time periods is indicated by the bar colour where darker colours reflects increased significance level. The thickness of the bar reflects the intensity of the wavelet spectrum, where thicker bar represents higher spectra at a given range of time periods. The estimated T_c (compensational time scale) separates the short time-period allogenic signals, which are only partially preserved in the record, from the long wavelength—signals, which are expected to be better preserved in the record.

explained by an indirect pathway of Nilotic sediment transport over the continental shelf along the coastline in addition to the deep basin route reaching the borehole directly from the Nile. This indirect pathway became effective during the Gelasian, when the Sinai-Israeli continental shelf has been built by margin parallel sediment transport processes (Ben Zeev & Gvirtzman, 2020; Schattner et al., 2015; Zucker et al., 2021). From this time forward the continental shelf has become a source of mass transport deposits such as the ISC (Schattnar et al., 2015). This secondary source could account for the enhanced deposition rate in the Sara borehole during the Gelasian.

6.2 | Oscillations in sand/shale ratio and their controls

The spectral analysis of GR depth series from the four boreholes of the Levant Basin show clear and pronounced oscillatory behaviour reflected by the increased spectral power of several key frequency bands that are consistent with the Milanković astronomical cycles. The wavelet analysis reveals increased power of specific frequency bands, particularly of long-wavelength periodicities although their statistical significance is lower (Figure 6, e.g., Tamar and Sara). We suggest that this could stem from the limited length of the studied records that can only contain a few long cycles, hence decreasing the statistical significance of these cycles due to the length of available records (Muller & MaCdonald, 2002).

Short periodicities that are often associated with environmental/allogenic forcing, are frequently shredded while sediments propagate through the transport system (Jerolmack & Paola, 2010). Thus, short-term signals in sedimentary records are strongly influenced by autogenic processes, such as channel avulsion and mobility (Straub et al., 2009; Wang et al., 2011). The time threshold (compensational time scale), below which allogenic-dominated signals are shredded, depends on the ratio between the vertical roughness, that is, channel depth, and the long-term basin-wide sedimentation rate (Straub et al., 2020). This threshold, termed compensation time scale, is defined as $T_c = \frac{l}{\bar{r}}$, where l is the roughness length (typical channel depth) and $\bar{r}$ is the long-term sedimentation rate (Wang et al., 2011).

Observed channels depth along the PQQ deposits of the Nile delta and slope are within a range of 10–40 m (Cross et al., 2009; Straub & Wang, 2013). A series of channels draining from the east delta towards the Levant Basin are also characterized by similar depth range of 10–50 (Gvirtzman et al., 2015) or 10–40 m (Zucker et al., 2017). The long-term sedimentation rate for calculating T_c varies significantly from the centre of the Nile Delta to the deep Levant Basin. A compilation of sedimentation rates for the Nile delta by Macgregor (2012) shows maximal values of 0.5–0.7 m/ky during the Pliocene. Sedimentation rates in the deep Levant Basin, on the other hand, were estimated by Zucker et al. (2021) to vary from 0.35 m/ky in the Gelasian to 0.07 m/ky in the Pleistocene based on isopach maps (Zucker et al., 2021). These estimates

are consistent with the specific values calculated for the boreholes studied here that vary from 0.05 m/ky (Tamar-1, Unit1) to 0.23 m/ky (Sara-1, Unit 2 including a slump). For estimating the shredding process, we take one value of 0.5 m/ky to represent deposition in the Nile delta and a second value of 0.15 m/ky to represent the deposition in the deep Levant Basin. Accordingly, for channel depth of 40 m, T_c is estimated to be 80 ky in the delta zone and 267 ky in the basin. For channel depth of 10 m, T_c is 20 ky in the delta zone and 67 ky in the basin. Because intensive signal shredding occurs mainly in the delta zone, T_c likely ranges between 20 and 80 ky. This means that in the Nile-Levant transport (and sedimentation) system, the preservation of allogenic oscillatory signals characterized by periodicities of tens of ky is less likely, while oscillatory signals of longer wavelength are expected to be preserved in the record. In practice, our spectral analyses indeed revealed weak precession and obliquity signals, a stronger short eccentricity signal, and a very strong long eccentricity signal. These observations suggest that short allogenic signals (10's ky) were almost completely shredded by autogenic processes, while longer oscillatory signals, 100 and 400 ky, were preserved in the record of the Nile-Levant system. Thus, our observations agree with the theoretical considerations regarding the shredding of environmental signals along source to sink systems.

Although eustatic fluctuations have a crucial role in controlling sand delivery and deposition in deep marine basins (Muto & Steel, 2002; Sweet et al., 2020; Zecchin et al., 2015), the magnitude of such fluctuations on time scales correspond to Milanković cycles became substantial only during the Quaternary, while during the Pliocene, which is the main part of this study, such fluctuation had smaller magnitude (Miller et al., 2005). Thus, we consider eustatic fluctuations to have had a minor role in controlling sand deposition in the Levant basin during the Pliocene–Gelasian, although the role of eustatic processes in shaping the studied record cannot be entirely ruled out. The observed oscillations in GR records closely match Milanković cycles (Riechers et al., 2022), which were suggested to pose the first-order control over Earth's climate systems during the Quaternary (e.g. Hays et al., 1976; Shackleton, 2000). Thus, the correspondence between previously described cycles and the current sedimentary record indicates that deposition in the Levant basin is substantially influenced by similar climatic drivers since the Pliocene. The main contributor of sediment to the Levant Basin is the Nile River, which receives most of its water and sediments from the Blue Nile draining the Ethiopian Plateau (Ahmed & Ismail, 2008; Eltahir, 1996), and is therefore likely to be affected by climatic fluctuations and orbital forcing (Grant et al., 2017; Rohling et al., 2015). Thus, based on the abovementioned findings, we suggest that there is a direct connection between the Nile outlet and the deep Levant Basin, which results in the recording of periodic signals as revealed by the increased spectral power of spectral bands matching Milanković cycles. Because sediments in the Levant Basin are mainly derived from the Nile, these results indicate that the Ethiopian Plateau experienced Milanković (−like) hydroclimatic oscillations during the PQ. Indeed, the ca. 400 ky oscillation is more pronounced and significant at Leviathan and Dolphin boreholes, which are more proximal to the Nile Delta (Figure 1b), and are, therefore directly influenced by the Nile River dynamics compared with the Tamar and Sara boreholes, which are located further away. In contrast, the 90–150 ky oscillation does not share a similar spatial pattern, and does not seem to correspond with borehole distance from the source. This oscillation is more pronounced in Sara, weaker in Tamar and Leviathan (although statistically significant) and is absent from Dolphin. Periodic components of shorter wave lengths, such as the 19–23 and 41 ky Milanković oscillations, which are characterized by lower spectral power in the record, may have still played a role in the Nile River source to sink system during the PQ, but are likely not well preserved in the record due to signal shredding.

6.3 | Processes controlling sand transport into the deep Levant basin

Sand proportion along the PQ sedimentary section in the deep Levant Basin is explained by two main processes: (i) A gradual long-term trend (10^3s ky) of increased sand supply, and (ii) short-term (10^0s–10^2s ky) oscillatory signals attributed to hydroclimatic processes in the Nile source.

6.3.1 | Long-term trends

The long-term trend is more pronounced in the Leviathan and Dolphin boreholes, which are closer to the Nile Delta. These boreholes contain many sandy units interbedded within the Pliocene–Gelasian section and a much thicker (170–100 m) upper sandy unit. In Sara and Tamar boreholes, the Pliocene–Gelasian sections contain less and thinner sandy units, and the upper sandy unit is 80–100 m thick. Noteworthy is the fact that the base of the upper sandy unit is diachronic: ca. 2.3 Ma in Leviathan, ca. 1.7 Ma in Dolphin, ca. 1.3 Ma in Tamar and ca. 1 Ma in Sara. We suggest that this indicates a progressive process

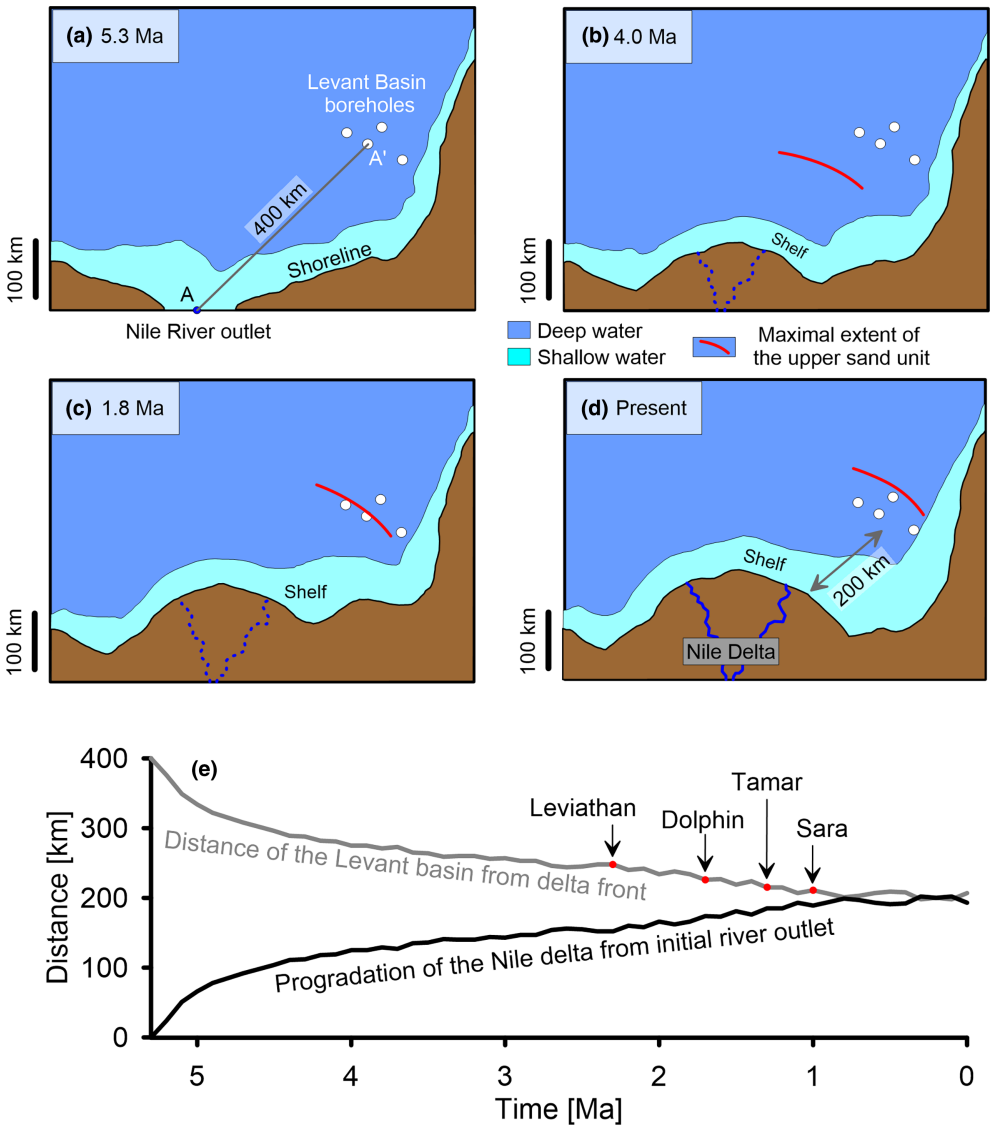

FIGURE 7 (a–d) Palaeogeographic evolution of the Eastern Mediterranean during the Pliocene–Quaternary (adapted from Zucker et al., 2021). (e) The distance from the delta front to the Levant basin since the Early Pliocene based on numerical simulation results from Zucker et al. (2021). During this time interval the Nile Delta prograded and the distance between the Nile outlet and the Levant basin shortened substantially, allowing larger sand volumes to reach the Levant Basin. The red dots indicate the age of the base of the upper sand unit at the four boreholes.

of sand supply into the deep basin, which first started in the proximity to the Nile mouth and then gradually propagated further north until it had finally formed a continuous sand sheet across the basin. These observations are in agreement with the accretion of the Nile Delta since the Early Pliocene, during which the distance between its edge and the studied deep basin boreholes became shorter by a half (Figure 7; Zucker et al., 2021). We suggest that sand supply into the deep basin has increased along with the propagating shelf edge as explained below. This agrees with the evidence supporting the development of turbidity channels alongside the Nile delta accretion as was recently revealed in 3D seismic data (Sagy et al., 2020).

6.3.2 | Short-term oscillations

We suggest that the 400–450 and 90–150 ky oscillations, which we interpret as representing the long and short eccentricity of the astronomical Milanković cycles (Hays et al., 1976; Riechers et al., 2022; Shackleton, 2000), were most likely driven by hydroclimatic fluctuations of the Nile River and particularly those of the Blue Nile that drains the Ethiopian Plateau. It is well established, since the very early studies on sediment transport in rivers, that the mobilization of particles of larger grain size requires higher transportation energy that is in general associated with higher water discharge and flow velocity (e.g. Hjulström, 1935).

Given the fact that sediment discharge at the Nile outlet depends on sediment availability, changes in provenance localities, erosion processes at the watershed and changes in vegetation cover, it is hard to determine whether wetter time intervals are associated with increasing sand/shale ratio or vice versa. Previous reconstructions of Nile delta sediment cores do not provide a clear picture of these relations as well. Revel et al. (2014) suggested that a peak in the Nile River outflow during the Early Holocene is associated with increased clay content based on an analysis of a sediment core offshore the Nile delta. In contrast, events of increased Blue Nile discharge were suggested to be associated with coarser grain size on average, based on another sediment core from the Nile delta (Blanchet et al., 2013). At this stage, further information about the hydrologic control on sand/shale ratio in the Nile River over longer time intervals and additional insights from mechanistic approaches are required to clarify this uncertainty.

6.3.3 | Sand transport from river mouth to deep basins

Sand is mostly distributed as water flow slows down in a variety of environments, ranging from river outlets to delta fronts. Then, at the delta front, it may be further transported by waves, tides, and floods (Goodbred & Saito, 2012; Kineke et al., 1996; Sternberg et al., 1996). In particular, sand is episodically transported (Dixon et al., 2012a, 2012b) by submarine turbidity currents that may travel over distances of hundreds of kilometres and arrive at deep remote basins (Babonneau et al., 2010; Fierens et al., 2019; Shanmugam et al., 1993; Strachan et al., 2016). However, even these strong episodic events are limited in their transport capabilities depending on a variety of conditions. We suggest that during the Pliocene, sand had reached the deep Levant Basin only during extreme episodic events due to the long distance between the Nile delta front and the Levant basin. However, as the Nile delta front propagated basinwards, sand supply into the Levant basin became more frequent and hence increased respectively until it had finally created the thick continuous upper unit (Figure 7a–d). Model simulations of sand delivery into the Levant Basin by Zucker et al. (2021) show that episodic sand deposition in the Levant Basin occurred when the distance of the Nile delta front from the deep Levant basin was 250–400 km (Figure 7e). Since the Early Pleistocene, as this distance became shorter, sand has been delivered continuously to the Levant Basin; first to the most proximal Leviathan borehole (ca. 2.3 Ma) and later on to the most distal Sara borehole (ca. 1 Ma). This means that only when the distance between the Nile delta front and the Levant Basin had shortened to less than ca. 250 km, large sand quantities were delivered to the Levant Basin. This model further emphasizes the Nile as the main source of sediments into the Levant Basin as was suggested previously (Steinberg et al., 2011; Zucker et al., 2020, 2021).

7 | SUMMARY AND CONCLUSIONS

By combining well-log data, 2D and 3D seismic surveys, statistical and time-series analyses, we present a framework for the accretion of sand-shale alternations in the deep Levant Basin during the PQ and their controls, with implications on the dynamics of the Nile River.

Highly variable sand proportion is observed along the four studied sections. This variability is characterized by: (i) a moderate long-term increase in sand proportion (at the Myr time scale), and (ii) short-term periodic fluctuations on the scale of 10s–100s ky. We interpret the long-term increase in sand proportion to reflect the progradation of the Nile Delta since the Early Pliocene. Delta progradation progressively supplied more Nilotic sand to the Levant Basin. Short-term fluctuations of sub-Milanković periodicities suggest that hydroclimatic dynamics of the Nile River further controlled sand deposition in the deep Levant Basin, 100 s of km north of the Nile outlet.

Spectral analyses of sand deposition during the Pliocene–Gelasian indicate pronounced power of periodicities in both the 90–150 and the ca. 400 ky bands, together with a weaker, yet statistically significant, component characterized by increased power at the 10's ky band. Thus, we interpret the increased power of these spectral bands to reflect hydroclimatic dynamics of the Nile River. The hydroclimatic control over sediment deposition at the Levant Basin indicates a direct connection between the Nile outlet, where the river discharges water and sediment, and the Levant Basin, where those sediments are deposited.

ACKNOWLEDGEMENTS

The authors thank Florencia Krawczyk, Jimmy Moneron and Yael Sagy for their assistance with the interpretation of the seismic data. We thank the BIRD foundation for their financial support. IS designed the research, analysed and interpreted the data and wrote the manuscript. YBD assisted in data curation, preparation, analyses and interpretation, wrote segments on data preparation and methodological aspects and edited the manuscript. ZG

supervised the research, edited the manuscript and acquired funding.

CONFLICT OF INTEREST STATEMENT

The authors have declared no conflict of interest.

DATA AVAILABILITY STATEMENT

The data that support the findings of this study are available from the corresponding author upon reasonable request.

ORCID

Ido Sirota https://orcid.org/0000-0001-5014-4369
Yoav Ben Dor https://orcid.org/0000-0002-5345-0297

REFERENCES

Ahmed, A. A., & Ismail, U. H. A. E. (2008). Sediment in the Nile River system. UNESCO-IHP-International Sediment Initiative, Khartoum, Sudan.

Atlas, B. (2002). *Introduction to wireline log analysis* (p. 312). Baker Hughes.

Babonneau, N., Cremer, M., & Bez, M. (2010). Sedimentary architecture in meanders of a submarine channel: Detailed study of the present Congo turbidite channel (zaiango project). *Journal of Sedimentary Research*, *80*, 852–866. https://doi.org/10.2110/jsr.2010.078

Bar, O., Zilberman, E., Feinstein, S., Calvo, R., & Gvirtzman, Z. (2016). The uplift history of the Arabian Plateau as inferred from geomorphologic analysis of its northwestern edge. *Tectonophysics*, *671*, 9–23. https://doi.org/10.1016/j.tecto.2016.01.004

Barber, P. M. (1981). Messinian subaerial erosion of the proto-Nile Delta. *Marine Geology*, *44*, 253–272.

Be'eri-Shlevin, Y., Avigad, D., Gerdes, A., & Zlatkin, O. (2014). Detrital zircon U-Pb-Hf systematics of Israeli coastal sands: New perspectives on the provenance of Nile sediments. *Journal of the Geological Society*, *171*, 107–116. https://doi.org/10.1144/jgs2012-151

Ben Dor, Y., Harlavan, Y., & Avigad, D. (2018). Provenance of the great Cambrian sandstone succession of northern Gondwana unravelled by strontium, neodymium and lead isotopes of feldspars and clays. *Sedimentology*, *65*(7), 2595–2620.

Ben Dor, Y., Marra, F., Armon, M., Enzel, Y., Brauer, A., Schwab, M. J., & Morin, E. (2021). Hydroclimatic variability of opposing Late Pleistocene climates in the Levant revealed by deep Dead Sea sediments. *Climate of the Past*, *17*, 2653–2677. https://doi.org/10.5194/cp-17-2653-2021

Ben Zeev, Y., & Gvirtzman, Z. (2020). When two salt tectonics systems meet: Gliding downslope the Levant margin and salt out-squeezing from under the Nile Delta. *Tectonics*, *39*, 1–24. https://doi.org/10.1029/2019TC005715

Blackman, R. B., & Tukey, J. W. (1958). The measurement of power spectra from the point of view of communications engineering—Part I. *Bell System Technical Journal*, *37*, 185–282.

Blanchet, C. L., Tjallingii, R., Frank, M., Lorenzen, J., Reitz, A., Brown, K., Feseker, T., & Brückmann, W. (2013). High-and low-latitude forcing of the Nile River regime during the Holocene inferred from laminated sediments of the Nile deep-sea fan. *Earth and Planetary Science Letters*, *364*, 98–110.

Bookman, R., Mor-Federman, T., Herut, B., Harlavan, Y., Taha, N., Stein, M., & Almogi-Labin, A. (2021). Development of the Nile Littoral cell during the past 8.2 kyr. *Quaternary Science Reviews*, *274*, 107262. https://doi.org/10.1016/j.quascirev.2021.107262

Clauzon, G., Suc, J.-P., Gautier, F., Berger, A., & Loutre, M.-F. (1996). Alternate interpretation of the Messinian salinity crisis: Controversy resolved? *Geology*, *24*, 363–366. https://doi.org/10.1130/0091-7613(1996)024<0363:AIOTMS>2.3.CO;2

Cross, N. E., Cunningham, A., Cook, R. J., Taha, A., Esmaie, E., & El Swidan, N. (2009). Three-dimensional seismic geomorphology of a deep-water slope-channel system: The Sequoia field, offshore west Nile Delta, Egypt. *AAPG Bulletin*, *93*(8), 1063–1086.

De Schepper, S., Gibbard, P. L., Salzmann, U., & Ehlers, J. (2014). A global synthesis of the marine and terrestrial evidence for glaciation during the Pliocene Epoch. *Earth-Science Reviews*, *135*, 83–102. https://doi.org/10.1016/j.earscirev.2014.04.003

Debret, M., Bout-Roumazeilles, V., Grousset, F., Desmet, M., McManus, J. F., Massei, N., Sebag, D., Petit, J. R., Copard, Y., & Trentesaux, A. (2007). The origin of the 1500-year climate cycles in Holocene north-Atlantic records. *Climate of the Past*, *3*, 569–575. https://doi.org/10.5194/cp-3-569-2007

Dixon, J. F., Steel, R. J., & Olariu, C. (2012a). River-dominated, shelf-edge deltas: Delivery of sand across the shelf break in the absence of slope incision. *Sedimentology*, *59*, 1133–1157. https://doi.org/10.1111/j.1365-3091.2011.01298.x

Dixon, J. F., Steel, R. J., & Olariu, C. (2012b). Shelf-edge delta regime as a predictor of deep-water deposition. *Journal of Sedimentary Research*, *82*, 681–687. https://doi.org/10.2110/jsr.2012.59

Donges, J. F., Donner, R. V., Trauth, M. H., Marwan, N., Schellnhuber, H. J., & Kurths, J. (2011). Nonlinear detection of paleoclimate-variability transitions possibly related to human evolution. *Proceedings of the National Academy of Sciences of the United States of America*, *108*, 20422–20427.

Elfassi, Y., Gvirtzman, Z., Katz, O., & Aharonov, E. (2019). Chronology of post-Messinian faulting along the Levant continental margin and its implications for salt tectonics. *Marine and Petroleum Geology*, *109*, 574–588. https://doi.org/10.1016/j.marpetgeo.2019.05.032

Ellis, D. V., & Singer, J. M. (2008). Well logging for earth scientists: v2. 389 p https://doi.org/10.1016/0920-4105(89)90013-2

Eltahir, E. A. B. (1996). El Nino and the natural variability in the flow of the Nile River. *Water Resources Research*, *32*, 131–137. https://doi.org/10.1029/95WR02968

Erba, E., Castradori, D., Guasti, G., & Ripepe, M. (1992). Calcareous nannofossils and Milankovitch cycles: The example of the Albian gault clay formation (southern England). *Palaeogeography, Palaeoclimatology, Palaeoecology*, *93*, 47–69.

Fang, J., Wu, H., Fang, Q., Shi, M., Zhang, S., Yang, T., Li, H., & Cao, L. (2020). Cyclostratigraphy of the global stratotype section and point (GSSP) of the basal Guzhangian stage of the Cambrian period. *Palaeogeography, Palaeoclimatology, Palaeoecology*, *540*, 109530. https://doi.org/10.1016/j.palaeo.2019.109530

Feng, Y. E., Yankelzon, A., Steinberg, J., & Reshef, M. (2016). Lithology and characteristics of the Messinian evaporite sequence of the deep Levant Basin, Eastern Mediterranean. *Marine Geology*, *376*, 118–131. https://doi.org/10.1016/j.margeo.2016.04.004

Fierens, R., Droz, L., Toucanne, S., Raisson, F., Jouet, G., Babonneau, N., Miramontes, E., Landurain, S., & Jorry, S. J. (2019). *Late quaternary geomorphology and sedimentary processes in the*

Zambezi turbidite system (Vol. *334*, pp. 1–28). Geomorphology. https://doi.org/10.1016/j.geomorph.2019.02.033

Gardosh, M., Druckman, Y., Buchbinder, B., & Calvo, R. (2008). The Oligo-Miocene deepwater system of the Levant Basin.

Garfunkel, Z. (1981). Internal structure of the Dead Sea leaky transform (rift) in relation to plate kinematics. *Tectonophysics*, *80*, 81–108. https://doi.org/10.1016/0040-1951(81)90143-8

Gargani, J., & Rigollet, C. (2007). Mediterranean Sea level variations during the Messinian salinity crisis. *Geophysical Research Letters*, *34*, 1–5. https://doi.org/10.1029/2007GL029885

Garzanti, E., Andò, S., Padoan, M., Vezzoli, G., & El Kammar, A. (2015). The modern Nile sediment system: Processes and products. *Quaternary Science Reviews*, *130*, 9–56. https://doi.org/10.1016/j.quascirev.2015.07.011

Garzanti, E., Andò, S., Vezzoli, G., Ali Abdel Megid, A., & El Kammar, A. (2006). Petrology of Nile River sands (Ethiopia and Sudan): Sediment budgets and erosion patterns. *Earth and Planetary Science Letters*, *252*, 327–341. https://doi.org/10.1016/j.epsl.2006.10.001

Garzanti, E., Vermeesch, P., Andò, S., Lustrino, M., Padoan, M., & Vezzoli, G. (2014). Ultra-long distance littoral transport of Orange sand and provenance of the Skeleton Coast Erg (Namibia). *Marine Geology*, *357*, 25–36. https://doi.org/10.1016/j.margeo.2014.07.005

Ghil, M., Allen, M., Dettinger, M., Ide, K., Kondrashov, D., Mann, M., Robertson, A. W., Saunders, A., Tian, Y., & Varadi, F. (2002). Advanced spectral methods for climatic time series. *Reviews of Geophysics*, *40*, 3-1–3-41. https://doi.org/10.1029/2000RG000092

Gong, C., Li, D., Steel, R. J., Peng, Y., Xu, S., & Wang, Y. (2021a). Delta-to-fan source-to-sink coupling as a fundamental control on the delivery of coarse clastics to deepwater: Insights from stratigraphic forward modelling. *Basin Research*, *33*, 2960–2983. https://doi.org/10.1111/bre.12591

Goodbred, S. L., & Saito, Y. (2012). Tide dominated deltas. In R. A. Davis & R. W. Dalrymple (Eds.), *Principles of tidal sedimentology* (pp. 129–151). Springer.

Grant, K. M., Rohling, E. J., Westerhold, T., Zabel, M., Heslop, D., Konijnendijk, T., & Lourens, L. (2017). A 3 million year index for North African humidity/aridity and the implication of potential pan-African humid periods. *Quaternary Science Reviews*, *171*, 100–118.

Grinsted, A., Moore, J. C., & Jevrejeva, S. (2004). Application of the cross wavelet transform and wavelet coherence to geophysical time series. *Nonlinear Processes in Geophysics*, *11*, 561–566.

Gvirtzman, G., & Buchbinder, B. (1978). The Late Tertiary of the cpastal plain and continental shelf of Israel, and its bearing on the history of the Eastern Mediterranean. *Initial Report*, *42*(2), 1195–1222.

Gvirtzman, Z., Csato, I., & Granjeon, D. (2014). Constraining sediment transport to deep marine basins through submarine channels: The Levant margin in the Late Cenozoic. *Marine Geology*, *347*, 12–26.

Gvirtzman, Z., Heida, H., Garcia-Castellanos, D., Bar, O., Zucker, E., & Enzel, Y. (2022). Limited Mediterranean sea-level drop during the Messinian salinity crisis inferred from the buried Nile canyon. *Communications Earth & Environment*, *3*(1), 216.

Gvirtzman, Z., Manzi, V., Calvo, R., Gavrieli, I., Gennari, R., Lugli, S., Reghizzi, M., & Roveri, M. (2017). Intra-Messinian truncation surface in the Levant Basin explained by subaqueous dissolution. *Geology*, *45*, 915–918. https://doi.org/10.1130/G39113.1

Gvirtzman, Z., Reshef, M., Buch-Leviatan, O., Groves-Gidney, G., Karcz, Z., Makovsky, Y., & Ben-Avraham, Z. (2015). Bathymetry of the Levant basin: Interaction of salt-tectonics and surficial mass movements. *Marine Geology*, *360*, 25–39.

Hajek, E. A., & Straub, K. M. (2017). Autogenic sedimentation in clastic stratigraphy. *Annual Review of Earth and Planetary Sciences*, *45*, 681–709.

Hays, J. D., Imbrie, J., & Shackleton, N. J. (1976). Variations in the earth's orbit: Pacemaker of the ice ages. *Science*, *194*, 1121–1132. https://doi.org/10.1126/science.194.4270.1121

Hilgen, F. J., & Langereis, C. G. (1989). Periodicities of $CaCO_3$ cycles in the Pliocene of Sicily: Discrepancies with the quasi-periods of the Earth's orbital cycles? *Terra Nova*, *1*, 409–415.

Hilgen, F. J., Hinnov, L. A., Abdul Aziz, H., Abels, H. A., Batenburg, S., Bosmans, J. H. C., de Boer, B., Hüsing, S. K., Kuiper, K. F., Lourens, L. J., Rivera, T., Tuenter, E., van de Wal, R. S. W., Wotzlaw, J. F., & Zeeden, C. (2015). Stratigraphic continuity and fragmentary sedimentation: The success of cyclostratigraphy as part of integrated stratigraphy. *Geological Society Special Publication*, *404*, 157–197. https://doi.org/10.1144/SP404.12

Hilgen, F. J., Lourens, L. J., Berger, A., Loutre, M. F., & De Louvain, C. (1993). Evaluation of the astronomically calibrated time scale for the Late Pliocene and earliest Pleistocene. *Paleoceanography*, *8*, 549–565.

Hjulström, F. (1935). *Studies of the morphological activity of rivers as illustrated by the River Fyris*. Doctoral dissertation, (p. 317). The Geological institution of the University of Upsala.

Imbrie, J., & Imbrie, J. Z. (1980). Modeling the climatic response to orbital variations. *Science*, *207*, 943–953. https://doi.org/10.1126/science.207.4434.943

Jerolmack, D. J., & Paola, C. (2010). Shredding of environmental signals by sediment transport. *Geophysical Research Letters*, *37*, 1–5. https://doi.org/10.1029/2010GL044638

Kelly, S. B. (1992). Milankovitch cyclicity recorded from Devonian non-marine sediments. *Terra Nova*, *4*, 578–584. https://doi.org/10.1111/j.1365-3121.1992.tb00599.x

Kineke, G. C., Sternberg, R. W., Trowbridge, J. H., & Geyer, W. R. (1996). Fluid-mud processes on the Amazon continental shelf. *Continental Shelf Research*, *16*, 667–696. https://doi.org/10.1016/0278-4343(95)00050-X

Kirkham, C., Bertoni, C., Cartwright, J., Lensky, N. G., Sirota, I., Rodriguez, K., & Hodgson, N. (2020). The demise of a 'salt giant' driven by uplift and thermal dissolution. *Earth and Planetary Science Letters*, *531*, 115933. https://doi.org/10.1016/j.epsl.2019.115933

Kondrashov, D., & Ghil, M. (2006). Spatio-temporal filling of missing points in geophysical data sets. *Nonlinear Processes in Geophysics*, *13*, 151–159. https://doi.org/10.5194/npg-13-151-2006

Krom, M. D., Cliff, R. A., Eijsink, L. M., Herut, B., & Chester, R. (1999). The characterisation of Saharan dusts and Nile particulate matter in surface sediments from the Levantine basin using Sr isotopes. *Marine Geology*, *155*, 319–330. https://doi.org/10.1016/S0025-3227(98)00130-3

Lau, K. M., & Weng, H. (1995). Climate signal detection using wavelet transform: How to make a time series sing. *Bulletin of the American Meteorological Society*, *76*(12), 2391–2402.

Lau, K. M., & Weng, H. (1995). Climate signal detection using wavelet transform: How to make a time series sing. *Bulletin of the American Meteorological Society*, *76*, 2391–2402. https://doi.org/10.1175/1520-0477(1995)076<2391:CSDUWT>2.0.CO;2

Liu, T., Ding, Z., & Rutter, N. (1999). Comparison of Milankovitch periods between continental loess and deep sea records over the last 2.5 Ma. *Quaternary Science Reviews*, *18*, 1205–1212. https://doi.org/10.1016/S0277-3791(98)00110-3

Lomb, N. R. (1976). Least-squares frequency analysis of unequally spaced data. *Astrophysics and Space Science*, *39*, 447–462. https://doi.org/10.1007/BF00648343

Lourens, L. J., Antonarakou, A., Hilgen, F. J., Van Hoof, A. A. M., & Zachariasse, W. J. (1996). Evaluation of the Plio-Pleistocene astronomical timescale. *Paleoceanography*, *11*, 391–413.

Macgregor, D. (2011). Rift shoulder source to Prodelta sink: The Cenozoic development of the Nile drainage system. *AAPG Search and Discover Article*, *50506*, 16.

Macgregor, D. S. (2012). The development of the Nile drainage system: Integration of onshore and offshore evidence. *Petroleum Geoscience*, *18*, 417–431. https://doi.org/10.1144/petgeo2011-074

Manzi, V., Gennari, R., Lugli, S., Persico, D., Reghizzi, M., Roveri, M., Schreiber, B. C., Calvo, R., Gavrieli, I., & Gvirtzman, Z. (2018). The onset of the Messinian salinity crisis in the deep Eastern Mediterranean basin. *Terra Nova*, *30*, 189–198. https://doi.org/10.1111/ter.12325

Marriner, N., Morhange, C., Borschneck, D., & Flaux, C. (2012). Holocene sedimentary sources in southern Lebanon, Eastern Mediterranean. *Quaternary International*, *266*, 105–116. https://doi.org/10.1016/j.quaint.2011.02.012

Martin, P. A., Lea, D. W., Rosenthal, Y., Shackleton, N. J., Sarnthein, M., & Papenfuss, T. (2002). Quaternary deep sea temperature histories derived from benthic foraminiferal Mg/Ca. *Earth and Planetary Science Letters*, *198*, 193–209. https://doi.org/10.1016/S0012-821X(02)00472-7

Martinez, J. F., Cartwright, J., & Hall, B. (2005). 3D seismic interpretation of slump complexes: Examples from the continental margin of Israel. *Basin Research*, *17*, 83–108.

Meyers, S. R., & Malinverno, A. (2018). Proterozoic Milankovitch cycles and the history of the solar system. *Proceedings of the National Academy of Sciences of the United States of America*, *115*, 6363–6368. https://doi.org/10.1073/pnas.1717689115

Miller, K. G., Kominz, M. A., Browning, J. V., Wright, J. D., Mountain, G. S., Katz, M. E., Sugarman, P. K., Cramer, B. S., Christie-Blick, N., & Pekar, S. F. (2005). The Phanerozoic record of global sea-level change. *Science*, *310*(5752), 1293–1298.

Moneron, J., & Gvirtzman, Z. (2022). Late Messinian submarine channel systems in the Levant Basin: Challenging the desiccation scenario. *Geology*, *50*(12), 1366–1371.

Mulder, T., & Cochonat, P. (1996). Classification of offshore mass movements. *Journal of Sedimentary Research*, *66*, 43–57.

Muller, R. A., & MaCdonald, G. G. (2002). *Ice ages and astronomical causes: Data, spectral analysis and mechanisms* (p. 274). Springer Science & Business Media.

Muto, T., & Steel, R. J. (2002). In defense of shelf-edge delta development during falling and lowstand of relative sea level. *Journal of Geology*, *110*, 421–436. https://doi.org/10.1086/340631

Needham, D. L., Pettingill, H. S., & Christensen, C. J. (2017). The Tamar giant gas field: Opening the subsalt Miocene gas play in the Levant Basin. *Giant Fields of the Decade*, 2000–2010. https://doi.org/10.1306/13572009M1133688

Nir, Y. (1984). *Recent sediments of the Israel Mediterranean continental shelf and slope* (p. 211). University of Gothenburg.

Niyazi, Y., Eruteya, O. E., Omosanya, K. O., Harishidayat, D., Johansen, S. E., & Waldmann, N. (2018). Seismic geomorphology of submarine channel-belt complexes in the Pliocene of the Levant Basin, offshore central Israel. *Marine Geology*, *403*, 123–138. https://doi.org/10.1016/j.margeo.2018.05.007

Pickering, K. T., Souter, C., Oba, T., Taira, A., Schaaf, M., & Platzman, E. (1999). Glacio-eustatic control on deep-marine clastic forearc sedimentation, Pliocene-mid-Pleistocene (c. 1180-600 ka) Kazusa Group, SE Japan. *Journal of the Geological Society*, *156*, 125–136. https://doi.org/10.1144/gsjgs.156.1.0125

Revel, M., Colin, C., Bernasconi, S., Combourieu-Nebout, N., Ducassou, E., Grousset, F. E., Rolland, Y., Migeon, S., Bosch, D., Brunet, P., Zhao, Y., & Mascle, J. (2014). 21,000 years of Ethiopian African monsoon variability recorded in sediments of the western Nile deep-sea fan. *Regional Environmental Change*, *14*, 1685–1696. https://doi.org/10.1007/s10113-014-0588-x

Riechers, K., Mitsui, T., Boers, N., & Ghil, M. (2022). Orbital insolation variations, intrinsic climate variability, and Quaternary glaciations. *Climate of the Past*, *18*, 863–893. https://doi.org/10.5194/cp-18-863-2022

Rohling, E. J., Marino, G., & Grant, K. M. (2015). Mediterranean climate and oceanography, and the periodic development of anoxic events (sapropels). *Earth-Science Reviews*, *143*, 62–97. https://doi.org/10.1016/j.earscirev.2015.01.008

Romans, B. W., Castelltort, S., Covault, J. A., Fildani, A., & Walsh, J. P. (2016). Environmental signal propagation in sedimentary systems across timescales. *Earth-Science Reviews*, *153*, 7–29.

Sagy, Y., Dror, O., Gardosh, M., & Reshef, M. (2020). The origin of the Pliocene to recent succession in the Levant basin and its depositional pattern, new insight on source to sink system. *Marine and Petroleum Geology*, *120*, 104540. https://doi.org/10.1016/j.marpetgeo.2020.104540

Said, R. (1981). *The geological evolution of the river Nile* (p. 151). Springer-Verlag.

Samuel, A., Kneller, B., Raslan, S., Sharp, A., & Parsons, C. (2003). Prolific deep-marine slope channels of the Nile Delta, Egypt. *AAPG Bulletin*, *87*(4), 541–560.

Schattner, U. (2021). Isolating the role of shore-parallel sediment transport in continental shelf build-up. *Continental Shelf Research*, *225*, 104480. https://doi.org/10.1016/j.csr.2021.104480

Schattner, U., & Lazar, M. (2016). Hierarchy of source-to-sink systems—Example from the Nile distribution across the eastern Mediterranean. *Sedimentary Geology*, *343*, 119–131. https://doi.org/10.1016/j.sedgeo.2016.08.006

Schattner, U., Gurevich, M., Kanari, M., & Lazar, M. (2015). Levant jet system—effect of post LGM seafloor currents on Nile sediment transport in the eastern Mediterranean. *Sedimentary Geology*, *329*, 28–39. https://doi.org/10.1016/j.sedgeo.2015.09.007

Schulte, J. A. (2016). Cumulative areawise testing in wavelet analysis and its application to geophysical time series. *Nonlinear Processes in Geophysics*, *23*, 45–57. https://doi.org/10.5194/npg-23-45-2016

Schulte, J. A. (2019). Statistical hypothesis testing in wavelet analysis: Theoretical developments and applications to Indian

rainfall. *Nonlinear Processes in Geophysics*, *26*, 91–108. https://doi.org/10.5194/npg-26-91-2019

Segev, A., Rybakov, M., Lyakhovsky, V., Hofstetter, A., Tibor, G., Goldshmidt, V., & Ben Avraham, Z. (2006). The structure, isostasy and gravity field of the Levant continental margin and the southeast Mediterranean area. *Tectonophysics*, *425*, 137–157. https://doi.org/10.1016/j.tecto.2006.07.010

Shackleton, N. J. (2000). The 100,000-year ice-age cycle identified and found to lag temperature, carbon dioxide, and orbital eccentricity. *Science*, *289*, 1897–1902. https://doi.org/10.1126/science.289.5486.1897

Shanmugam, G., Spalding, T. D., & Rofheart, D. H. (1993). Process sedimentology and reservoir quality of deep marine bottom currents reqorked sands (sandy contourites): An example from the Gulf of Mexico. *AAPG Bulletin*, *77*, 1241–1259.

Steinberg, J., Gvirtzman, Z., Folkman, Y., & Garfunkel, Z. (2011). Origin and nature of the rapid late Tertiary filling of the Levant Basin. *Geology*, *39*, 355–358. https://doi.org/10.1130/G31615.1

Sternberg, R. W., Cacchione, D. A., Paulson, B., Kineke, G. C., & Drake, D. E. (1996). Observations of sediment transport on the Amazon subaqueous delta. *Continental Shelf Research*, *16*, 697–715. https://doi.org/10.1016/0278-4343(95)00045-3

Stow, D., & Smillie, Z. (2020). Distinguishing between deep-water sediment facies: Turbidites, contourites and hemipelagites. *Geosciences (Switzerland)*, *10*, 1–43. https://doi.org/10.3390/geosciences10020068

Strachan, L. J., Bostock, H. C., Barnes, P. M., Neil, H. L., & Gosling, M. (2016). Non-cohesive silt turbidity current flow processes; insights from proximal sandy-silt and silty-sand turbidites, Fiordland, New Zealand. *Sedimentary Geology*, *342*, 118–132. https://doi.org/10.1016/j.sedgeo.2016.06.017

Stratford, K., Williams, R. G., & Myers, P. G. (2000). Impact of the circulation on sapropel formation in the eastern Mediterranean. *Global Biogeochemical Cycles*, *14*, 683–695.

Straub, K. M., & Wang, Y. (2013). Influence of water and sediment supply on the long-term evolution of alluvial fans and deltas: Statistical characterization of basin-filling sedimentation patterns. *Journal of Geophysical Research: Earth Surface*, *118*(3), 1602–1616.

Straub, K. M., Duller, R. A., Foreman, B. Z., & Hajek, E. A. (2020). Buffered, incomplete, and shredded: The challenges of reading an imperfect stratigraphic record. *Journal of Geophysical Research: Earth Surface*, *125*(3), e2019JF005079.

Straub, K. M., Paola, C., Mohrig, D., Wolinsky, M. A., & George, T. (2009). Compensational stacking of channelized sedimentary deposits. *Journal of Sedimentary Research*, *79*, 673–688. https://doi.org/10.2110/jsr.2009.070

Sutcliffe, J. V., & Parks, Y. P. (1999). The hydrology of the Nile. IAHS Special Publication No. 5, v. 5.

Sweet, M. L., Gaillot, G. T., Jouet, G., Rittenour, T. M., Toucanne, S., Marsset, T., & Blum, M. D. (2020). Sediment routing from shelf to basin floor in the Quaternary Golo system of Eastern Corsica, France, western Mediterranean Sea. *Bulletin*, *132*(5–6), 1217–1234.

Torfstein, A., & Steinberg, J. (2020). The Oligo-Miocene closure of the Tethys Ocean and evolution of the proto-Mediterranean Sea. *Scientific Reports*, *10*, 1–10. https://doi.org/10.1038/s41598-020-70652-4

Torrence, C., & Compo, G. P. (1998). A practical guide to wavelet analysis. *Bulletin of the American Meteorological Society*, *79*, 61–78. https://doi.org/10.1175/1520-0477(1998)079<0061:APGTWA>2.0.CO;2

Trauth, M. H. (2021). Spectral analysis in Quaternary sciences. *Quaternary Science Reviews*, *270*, 107157. https://doi.org/10.1016/j.quascirev.2021.107157

Venkatarathnam, K., & Ryan, W. B. F. (1971). Dispersal patterns of clay minerals in the sediments of the eastern Mediterranean Sea. *Marine Geology*, *11*, 261–282.

Waltham, D. (2015). Milankovitch period uncertainties and their impact on cyclostratigraphy. *Journal of Sedimentary Research*, *85*, 990–998. https://doi.org/10.2110/jsr.2015.66

Wang, Y., Straub, K. M., & Hajek, E. A. (2011). Scale-dependent compensational stacking: An estimate of autogenic time scales in channelized sedimentary deposits. *Geology*, *39*, 811–814. https://doi.org/10.1130/G32068.1

Weedon, G. P., & Jenkyns, H. C. (1999). Cyclostratigraphy and the Early Jurassic timescale: Data from the Belemnite Marls, Dorset, Southern England. *Bulletin of the Geological Society of America*, *111*, 1823–1840. https://doi.org/10.1130/0016-7606(1999)111<1823:CATEJT>2.3.CO;2

Weedon, G. P., Jenkyns, H. C., Coe, A. L., & Hesselbo, S. P. (1999). Astronomical calibration of the Jurassic time-scale from cyclostratigraphy in British mudrock formations. *Philosophical Transactions of the Royal Society A: Mathematical, Physical and Engineering Sciences*, *357*, 1787–1813. https://doi.org/10.1098/rsta.1999.0401

Welch, P. D. (1967). The use of fast Fourier transform for the estimation of power spectra: A method based on time averaging over short, modified periodograms. *IEEE Transactions on Audio and Electroacoustics*, *15*, 70–73. https://doi.org/10.1109/TAU.1967.1161901

Weldeab, S., Emeis, K. C., Hemleben, C., & Siebel, W. (2002). Provenance of lithogenic surface sediments and pathways of riverine suspended matter in the eastern Mediterranean Sea: Evidence from $^{143}Nd/^{144}Nd$ and $^{87}Sr/^{86}Sr$ ratios. *Chemical Geology*, *186*, 139–149. https://doi.org/10.1016/S0009-2541(01)00415-6

Witt, A., & Schumann, A. Y. (2005). Holocene climate variability on millennial scales recorded in Greenland ice cores. *Nonlinear Processes in Geophysics*, *12*, 345–352.

Wu, H., Zhang, S., Feng, Q., Jiang, G., Li, H., & Yang, T. (2012). Milankovitch and sub-Milankovitch cycles of the early Triassic Daye formation, South China and their geochronological and paleoclimatic implications. *Gondwana Research*, *22*, 748–759. https://doi.org/10.1016/j.gr.2011.12.003

Zachos, J., Pagani, M., Sloan, L., Thomas, E., & Billups, K. (2001). Trends, rhythms, and aberrations in global climate 65 Ma to present. *Science*, *292*, 686–693.

Zecchin, M., Ceramicola, S., Lodolo, E., Casalbore, D., & Chiocci, F. L. (2015). Episodic, rapid sea-level rises on the central Mediterranean shelves after the Last Glacial Maximum: A review. *Marine Geology*, *369*, 212–223. https://doi.org/10.1016/j.margeo.2015.09.002

Zilberman, E., & Calvo, R. (2013). Remnants of Miocene fluvial sediments in the Negev Desert, Israel, and the Jordanian Plateau: Evidence for an extensive subsiding basin in the northwestern margins of the Arabian plate. *Journal of African Earth Sciences*, *82*, 33–53. https://doi.org/10.1016/j.jafrearsci.2013.02.006

Zucker, E., Gvirtzman, Z., Granjeon, D., Garcia-Castellanos, D., & Enzel, Y. (2021). The accretion of the Levant continental shelf alongside the Nile Delta by immense margin-parallel sediment

transport. *Marine and Petroleum Geology*, *126*, 104876. https://doi.org/10.1016/j.marpetgeo.2020.104876

Zucker, E., Gvirtzman, Z., Steinberg, J., & Enzel, Y. (2017). Diversion and morphology of submarine channels in response to regional slopes and localized salt tectonics, Levant Basin. *Marine and Petroleum Geology*, *81*, 98–111.

Zucker, E., Gvirtzman, Z., Steinberg, J., & Enzel, Y. (2020). Salt tectonics in the eastern Mediterranean Sea: Where a giant delta meets a salt giant. *Geology*, *48*, 134–138. https://doi.org/10.1130/G47031.1

How to cite this article: Sirota, I., Ben Dor, Y., & Gvirtzman, Z. (2024). Short-term climatic oscillations versus long-term delta propagation: Controls on sand transport into the deep Levant Basin since the Pliocene. *Basin Research*, *36*, e12892. https://doi.org/10.1111/bre.12892